Journal of Ovonic Research Vol. 21, No. 2, March - April 2025, p. 225 - 234

Study of spinel $ZnNi_xMn_xCo_{2-2x}O_4$ (x = 0, 0.25, 0.5, 0.75, and 1.0) nanomaterials for supercapacitor electrode applications by hydrothermal synthesis

T. Singha [a], T. Kansaard [a], Y. Chuminjak [b], N. Pijarn [c], S. Intarasiri [a],
S. Wannapop [a], A. Somdee [a,*]
[a] *Faculty of Science, Energy, and Environment, King Mongkut's University of Technology North Bangkok, Rayong Campus, Rayong 21120, Thailand*
[b] *Energy Storage Technology Research Team (ESTT), National Energy Technology Center (ENTEC), National Science and Technology Development Agency (NSTDA), 111 Thailand Science Park, Thanon Phahonyothin, Tambon Klong Nueng, Amphoe Klong Luang, Pathum Thani 12120, Thailand*
[c] *Department of Chemistry, Faculty of Science, Ubon Ratchathani University, Mueang Si Khi, Warin Chamrab, Ubon Ratchathani, 34190, Thailand*

This research investigated the properties and performance of spinel $ZnNi_xMn_xCo_{2-2x}O_4$ for use as a supercapacitor electrode. All materials employed a single-step hydrothermal procedure to synthesize. The stoichiometric values of x = 0, 0.25, 0.50, 0.75, and 1.0 were studied. Various characterized methods, e.g., XRD, SEM, and XPS, were utilized for material characterization. The electrode properties were assessed with a 2 M KOH electrolyte as the testing medium. For the electrochemical studies in this work, cyclic voltammetry (CV) was used to analyze the type of material being a supercapacitor, where the result indicated the spinel $ZnNi_xMn_xCo_{2-2x}O_4$ exhibited the pseudocapacitor type. Furthermore, the charging and discharging of the supercapacitor were employed to examine the absorption and desorption of charges at the charging and discharging process, respectively. The internal resistance of the electrode, which affects the supercapacitor's efficiency, was evaluated using electrochemical impedance spectroscopy (EIS). Among those CV studies, the electrode made from the $ZnNi_{0.75}Mn_{0.75}Co_{0.5}O_4$ material showed the best supercapacitor property, demonstrating a capacitance of 535 F/g at 5 mV/s scan rate.

(Received January 11, 2025; Accepted April 4, 2025)

Keywords: Supercapacitor, Hydrothermal method, Nanomaterial, Spinel oxides

1. Introduction

The fatigue caused by reliance on fossil fuels has wide-ranging impacts on the environment and society, leading to the pursuit of renewable energy sources. However, due to the variability and unpredictability of natural energy sources, energy storage solutions are necessary to store energy. At the same time, it is being produced to guarantee a sustainable supply. Many forms of energy can be stored, such as heat, solar, gravitational, electrochemical, and electricity. In the case of electrochemical and electrical energy storage, batteries and supercapacitors have garnered much attention for many technological applications. When comparing these two types of energy storage, supercapacitors have been dominant due to their high-speed charge and discharged capabilities at high current ratings, long capacitance retention, and low resistance [1–5].

Supercapacitors may be divided into three types depending on their faradaic interaction. This research focused on the pseudocapacitor type of supercapacitor that uses metal oxides as electrode materials [6–10]. The three types of supercapacitors differ based on the materials used for the electrodes. Materials derived from carbon, including activated carbon, graphene, graphene oxide, and carbon nanotubes, exhibited the characteristics of electrical double-layer capacitors (EDLCs). In contrast, metal oxides, sulfides, and similar compounds are typically used in pseudocapacitors (PDSs) and hybrid supercapacitors.

---

[*] Corresponding author: asanee.s@sciee.kmutnb.ac.th

https://doi.org/10.15251/JOR.2025.212.225

Transition metals are widely studied for use in supercapacitor materials due to their ability to enhance performance while being low-cost and stable over the long term. Among various metal oxide materials, the spinel-type structure, the chemical formula AB_2O_4, is fascinating. According to the formula AB_2O_4, A represents a metal cation with a +2 valency, while B represents a metal cation with a +3 valency. Metal oxides, namely $NiCo_2O_4$, $CuCo_2O_4$, $MnCo_2O_4$, and $ZnCo_2O_4$, are extensively researched due to their low production costs and high theoretical capacitance [11–23]. For example, A. J. C. Mary et al. synthesized $ZnCo_2O_4$ doped with Mn using a hydrothermal method, achieving a capacitance of 707.4 F/g using the electrolyte of 2 M KOH [24]. Similarly, M. Sharma et al. synthesized zinc cobalt oxide ($Zn_{1-x}Cu_xCo_2O_4$) with Cu doping using a hydrothermal method, resulting in the most significant capacitance of 1,425 F/g using 6 M KOH as an electrolyte [25].

In this research, spinel $ZnNi_xMn_xCo_{2-2x}O_4$ nanocomposites were synthesized with x values of 0, 0.25, 0.50, 0.75, and 1.0. All materials were prepared through a single-step hydrothermal approach. Various characterization methods were applied, including XRD, SEM, TEM, and XPS. Electrochemical properties of the electrode materials coated were assessed by the CV, GCD, and EIS.

2. Experiment

2.1 Sample preparations

The precursor for $ZnNi_xMn_xCo_{2-2x}O_4$ at different stoichiometric ratios was prepared according to the specified x values: 0, 0.25, 0.50, 0.75, and 1.0. This work used metal acetate, e.g., Zn, Ni, Co, and Mn acetate, as started material precursors. For x = 0, the expected material was spinel $ZnCo_2O_4$. A 5 mmol of zinc acetate dihydrate was dissolved in 50 mL DI water and stirred for 15 min until fully dissolved. After that, 10 mmol of cobalt acetate tetrahydrate was added to the previous Zn^{2+} solution. The mixed solution was further stirred for 15 minutes. Then, 10 mL NaOH (3 M) was slowly dropwise to the Zn and Co mixing solutions and stirred for 1 hour. The pre-precipitate was transferred into a 100 mL hydrothermal reactor. Then, it was autoclaved at 160 °C for 10 hours. When the reaction cooled down, the material was washed with DI and dried in an electrical oven (60 °C, 24 hours). Subsequently, the products were calcined at 800 °C for 2 hours. The other stoichiometric ratios (x = 0.25, 0.5, 0.75, and 1.0) were done similarly to the x = 0, where the synthesis diagram is summarized in Fig. 1.

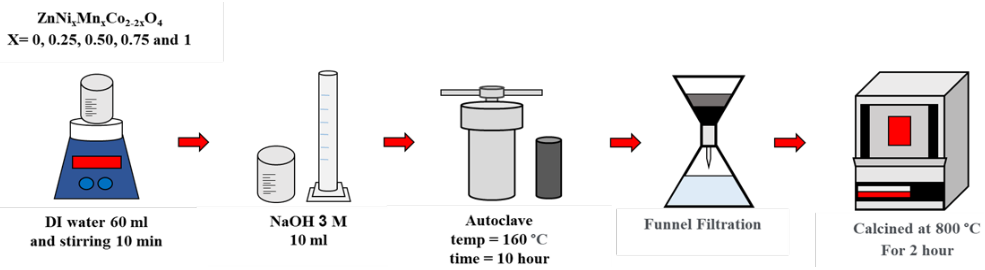

Fig. 1. Synthesis diagram of $ZnNi_xMn_xCo_{2-2x}O_4$ at x = 0, 0.25, 0.50, 0.75, and 1.0.

2.2. Characterizations

The prepared samples were analyzed for their crystalline structure using XRD (Bruker D8 eco) scanning covering a range of 15° to 80°. The morphology and surface characteristics of all spinel-type structures were analyzed using SEM (JEOL, JSM IT800) and TEM (JEOL, JEM 2100 Plus). Additionally, the elemental analysis was performed with XPS (KRATOS, Axis Ultra DLD).

2.3. Photoelectrochemical performances

The material paste for coating on an electrode was prepared using a highly conductive carbon addition, N-methyl-2-pyrrolidone (NMP) solvent, and poly(vinylidene fluoride) (PVDF) binder in a weight ratio of 8:1:1, respectively. The spinel paste was coated onto a nickel sheet foam substrate, where the control coating area was ~1 cm^2. The specimen was dried in a general electrical oven at 80 °C for 24 hours. The electrochemical performance was studied only in a three-electrode method, where 2 M KOH was applied as the electrolyte. The CV experiment potential was conducted at –0.5 to +0.5 V vs. an Ag/AgCl reference electrode. The cell electrode was connected as a working electrode, while a Pt was applied as the counter electrode. Many scan rates determined the electrodes' performance, ranging from 5 mV/s to 100 mV/s. The specific capacitance (Cs) was calculated by the following equation:

$$Cs = \frac{\int IdV}{m \times v \times \Delta V} \tag{1}$$

where $\int IdV$ is the absolute area obtained from the CV experiment, m is the loaded mass of the active material coated on a nickel foam electrode, v is the CV scan rate, and ΔV is the potential difference. GCD tests were performed at current densities between 3 and 25 mA/cm², with the voltage scan limited to 0 to 0.5 V. EIS measurements were studied over a frequency range from 0.1 Hz to 10^5 Hz and a 10 mV AC signal.

3. Result and discussion

Fig. 2 shows the XRD patterns in the 2θ scan range from 15° to 80° for samples representing different values of x. The sample analysis with x = 0 indicated a composite of $ZnCo_2O_4$ and ZnO phases. The XRD peaks located at 18.9°, 31.2°, 36.8°, 38.5°, 44.7°, 59.3°, and 65.2° were assigned to $ZnCo_2O_4$ and corresponded to the (111), (220), (311), (222), (400), (511), and (440) planes, respectively, as confirmed by PDF card 00-023-1390 [37]. The peaks located at 31.8°, 34.4°, 36.3°, 47.5°, 56.6°, and 62.9° were associated with the ZnO phase. Compared to the PDF card 01-089-7102 [38], these peaks were assigned as the plane indices of (100), (002), (101), (102), (110), and (103), respectively.

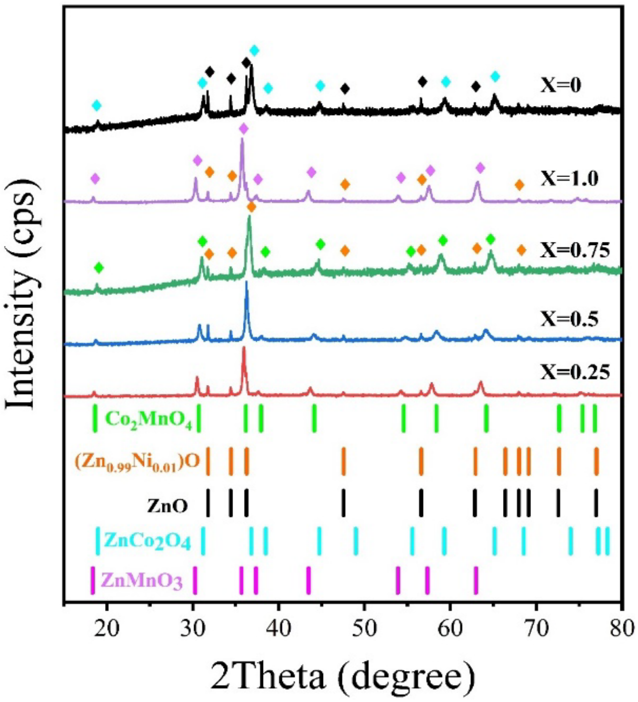

Fig. 2. XRD patterns of various spinel $ZnNi_xMn_xCo_{2-2x}O_4$ samples, with x = 0, 0.25, 0.5, 0.75, and 1.0).

In the case of x = 1.0, the XRD analysis of $ZnNiMnO_4$ revealed phases of $ZnMnO_3$ and $Zn_{0.99}Ni_{0.01}O$ according to PDF card 01-070-6709 [39] and PDF card 01-078-3344 [40], respectively. The diffraction peaks for the $ZnMnO_3$ phase were located at 18.4°, 30.3°, 35.6°, 37.4°, 43.5°, 53.8°, 57.3°, and 62.9°, corresponding to the indices of (111), (220), (311), (222), (400), (422), (511), and (440). The diffraction peaks for the $Zn_{0.99}Ni_{0.01}O$ phase were located at 31.7°, 34.5°, 47.6°, 56.6°, and 68.0°, which correspond to the planes (100), (002), (102), (110), and (112), respectively.

The XRD pattern for stoichiometric ratios of x = 0.25, 0.5, and 0.75 showed similar characteristics. When compared to the database, these three materials were found to be comprised of $Zn_{0.99}Ni_{0.01}O$ and Co_2MnO_4 phases (PDF card 00-001-1130) [41]. The peaks located at 31.7°, 34.5°, 36.3°, 47.6°, 56.6°, 62.9°, and 67.9° were attributed to the $Zn_{0.99}Ni_{0.01}O$ phase, while the other diffraction peak located at 18.6°, 30.7°, 37.9°, 44.1°, 54.6°, 58.4°, 64.2°, and 75.4° were indexed to Co_2MnO_4, assigning as the planes (111), (220), (222), (400), (422), (511), (440), and (541), respectively.

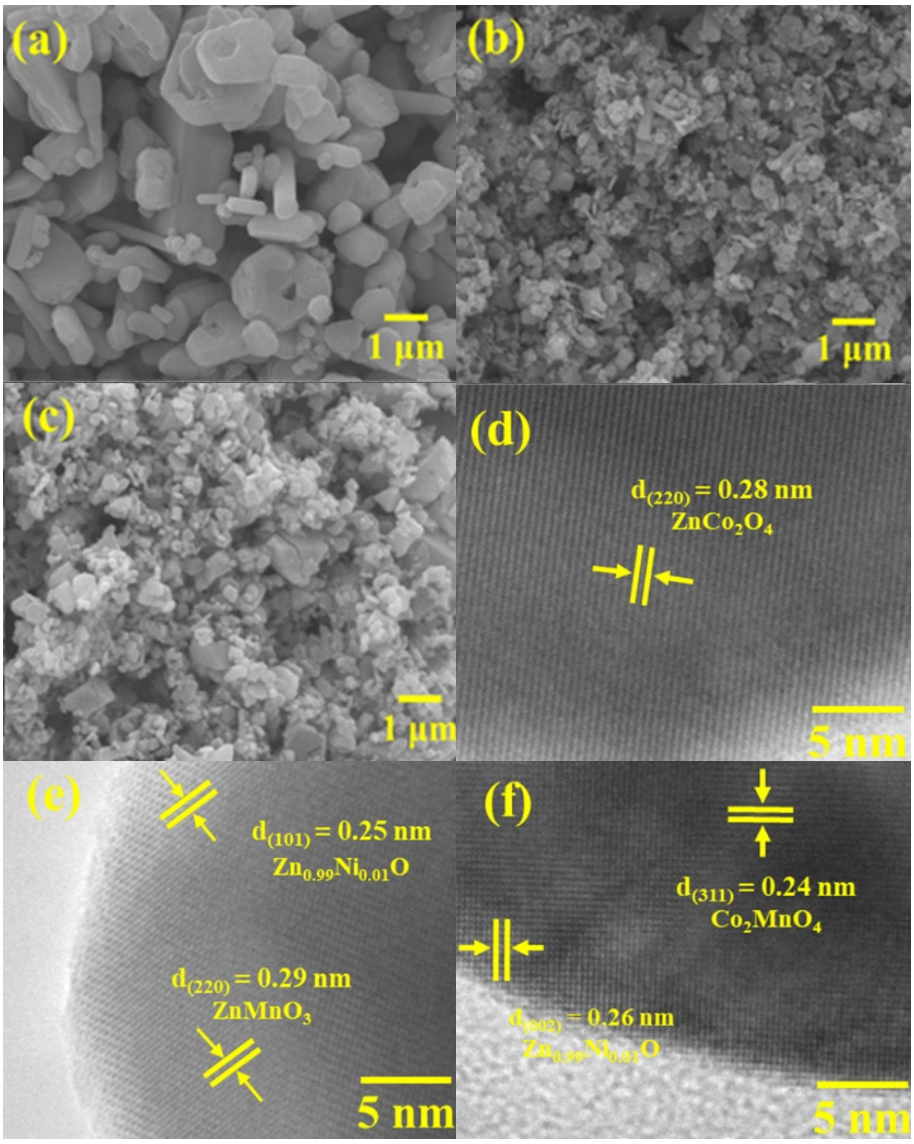

Fig. 3. SEM images represent of (a) $ZnCo_2O_4$, (b) $ZnNiMnO_4$, and (c) $ZnNi_{0.75}Mn_{0.75}Co_{0.5}O_4$ and TEM images of (d) $ZnCo_2O_4$, (e) $ZnNiMnO_4$, and (f) $ZnNi_{0.75}Mn_{0.75}Co_{0.5}O_4$.

Fig. 3 displays the selected samples' SEM images. In Fig. 3(a), the morphology of $ZnCo_2O_4$ displays hexagonal nanorods and nanoplate structures, indicating the presence of at least two mixed phases. In Fig. 3(b) and Fig. 3(c), the morphology of the $ZnNiMnO_4$ and $ZnNi_{0.75}Mn_{0.75}Co_{0.5}O_4$

samples is more difficult to identify using SEM. Notably, the particle sizes of $ZnNiMnO_4$ and $ZnNi_{0.75}Mn_{0.75}Co_{0.5}O_4$ appear smaller than $ZnCo_2O_4$, suggesting that smaller particle size correlates with a larger surface area.

TEM images of $ZnCo_2O_4$, $ZnNiMnO_4$, and $ZnNi_{0.75}Mn_{0.75}Co_{0.5}O_4$ are depicted in Fig. 3(d), Fig. 3(e), and Fig. 3(f), respectively. In Fig. 3(d), the interplanar d-spacing of $ZnCo_2O_4$ is observed, with a lattice distance of 0.28 nm that corresponds well to the plane (220) of $ZnCo_2O_4$. Fig. 3(e) shows the heterostructure of $Zn_{0.99}Ni_{0.01}O$ and $ZnMnO_3$. The d-spacing of 0.25 nm matches the (101) plane of $Zn_{0.99}Ni_{0.01}O$, while the d-spacing of 0.29 nm originates from the Miller plane of (220) reflection of $ZnMnO_3$. In Fig. 3(f), two phases are mixed: Co_2MnO_4 and $Zn_{0.99}Ni_{0.01}O$. The 0.24 nm d-spacing corresponds to the (311) Co_2MnO_4 phase, whereas the 0.26 nm lattice d-spacing is attributed to the (002) $Zn_{0.99}Ni_{0.01}O$ phase.

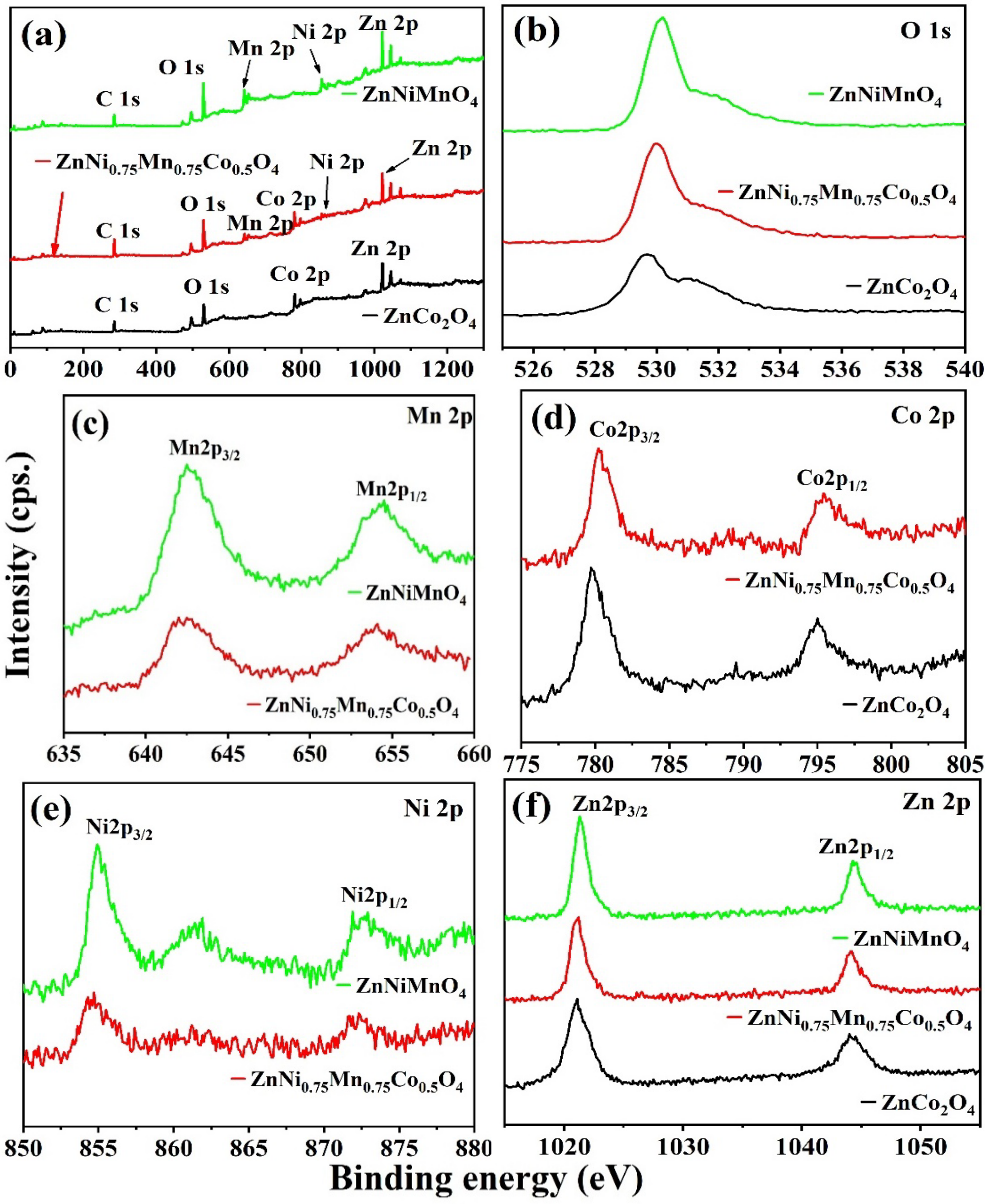

Fig. 4. XPS spectra of $ZnCo_2O_4$, $ZnNiMnO_4$, and $ZnNi_{0.75}Mn_{0.75}Co_{0.5}O_4$: (a) survey XPS scan, (b) O 1s, (c) Mn 2p, (d) Co 2p, (e) Ni 2p, and (f) Zn 2p.

Fig. 4 shows the XPS spectra of $ZnCo_2O_4$, $ZnNiMnO_4$, and $ZnNi_{0.75}Mn_{0.75}Co_{0.5}O_4$ nanocomposites. The survey chemical composition of each material is shown in Fig. 4(a). For the O 1 spectra, the O 1s of $ZnNiMnO_4$ were similar to that of $ZnNi_{0.75}Mn_{0.75}Co_{0.5}O_4$. However, a shift in the O 1s spectrum was observed for $ZnCo_2O_4$ compared to the other two samples, suggesting that the oxygen in $ZnCo_2O_4$ interacts more strongly with the Co atom than in the other materials. For the remaining elements, the shifts in the XPS peaks exhibited similar trends.

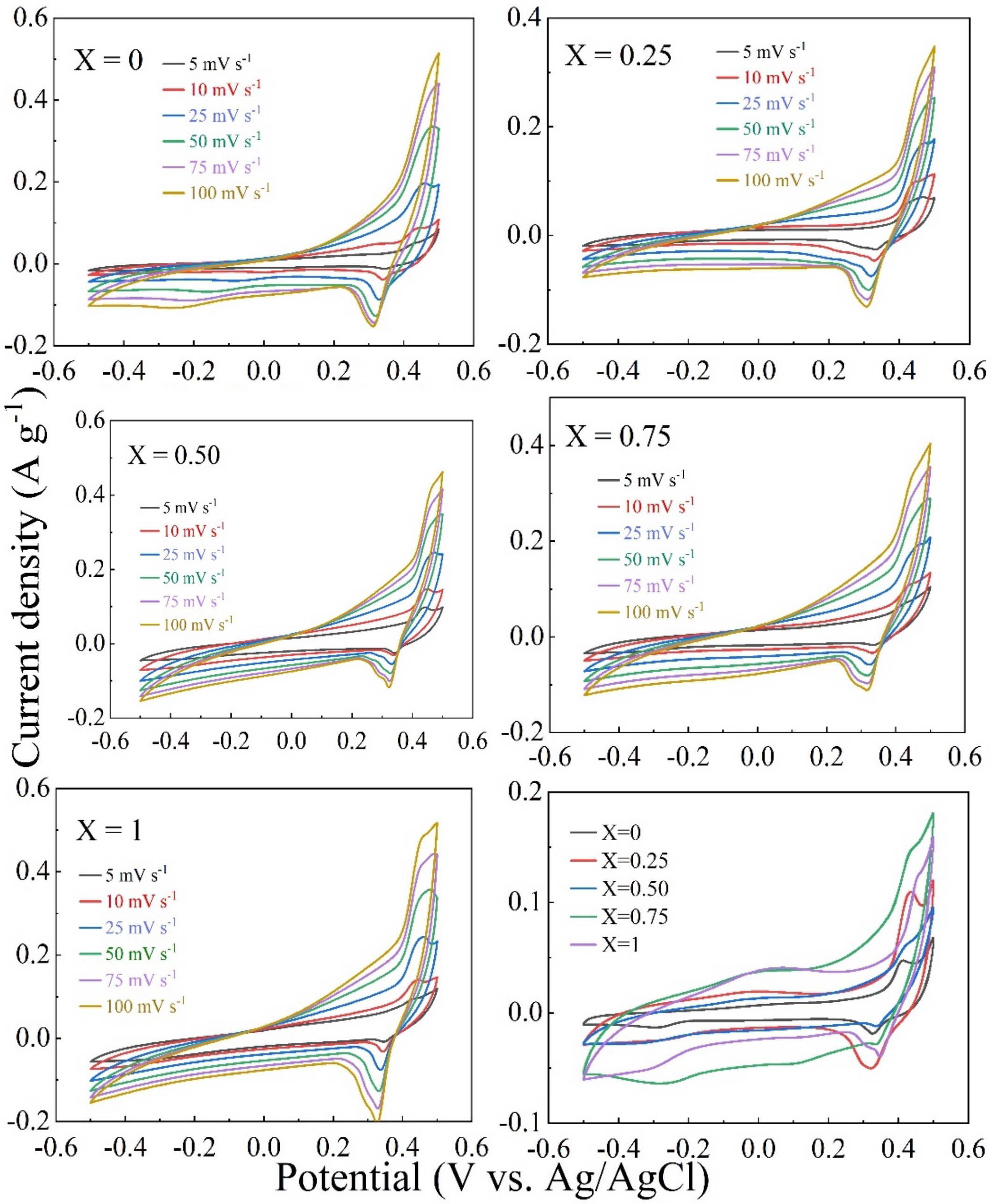

Fig. 5. CV curves of different materials of spinel $ZnNi_xMn_xCo_{2-2x}O_4$ (x = 0, 0.25, 0.5, 0.75, and 1.0) and comparative material at a scan rate of 5 mV/s.

Electrode performance was evaluated using CV technique. In the three-electrode study, all material's CV curves are depicted in Fig. 5. The potential window range studied was scanned from –0.5 to +0.5 V. The results revealed the redox peaks of each sample, indicating pseudocapacitive characteristics [42]. For comparison purposes, the CV results at 5 mV/s were summarized in Fig. 5(f). By integrating the CV curve, the ZnNi0.$_{75}$Mn$_{0.75}$Co$_{0.5}$O$_4$ area was larger than all materials studied in this work. The area increase is attributed to the variation of Co, Ni, and Mn substituent atoms at different stoichiometric ratios. The calculated specific charge storage capacity for the material at varying scan rates is summarized in Table 1.

Table 1. Calculate the specific capacitance of each material.

Scan rate (mV/s)	**Specific capacitance (F/g)**				
	x = 0	x = 1	x = 0.25	x = 0.50	x = 0.75
5	88.72	533.86	184.15	181.31	535.09
10	83.56	413.01	165.11	126.73	415.68
25	69.98	276.45	113.62	77.57	268.09
50	55.07	191.51	75.70	52.95	176.01
75	46.41	151.38	58.44	42.28	133.05
100	40.67	126.34	47.95	35.99	107.47

Fig. 6 compares the material's charge and discharge efficiency coated on the electrode at applied currents of 3, 5, and 10 mA/cm². The voltage range examined was from 0 V to +0.5 V. It is noteworthy that the charging period was not well balanced with the discharging time, leading to poor GCD results. However, in Fig. 6(f), when comparing all GCD results, $ZnNi_{0.75}Mn_{0.75}Co_{0.5}O_4$ exhibited the best performance. The GCD results align with the CV tests.

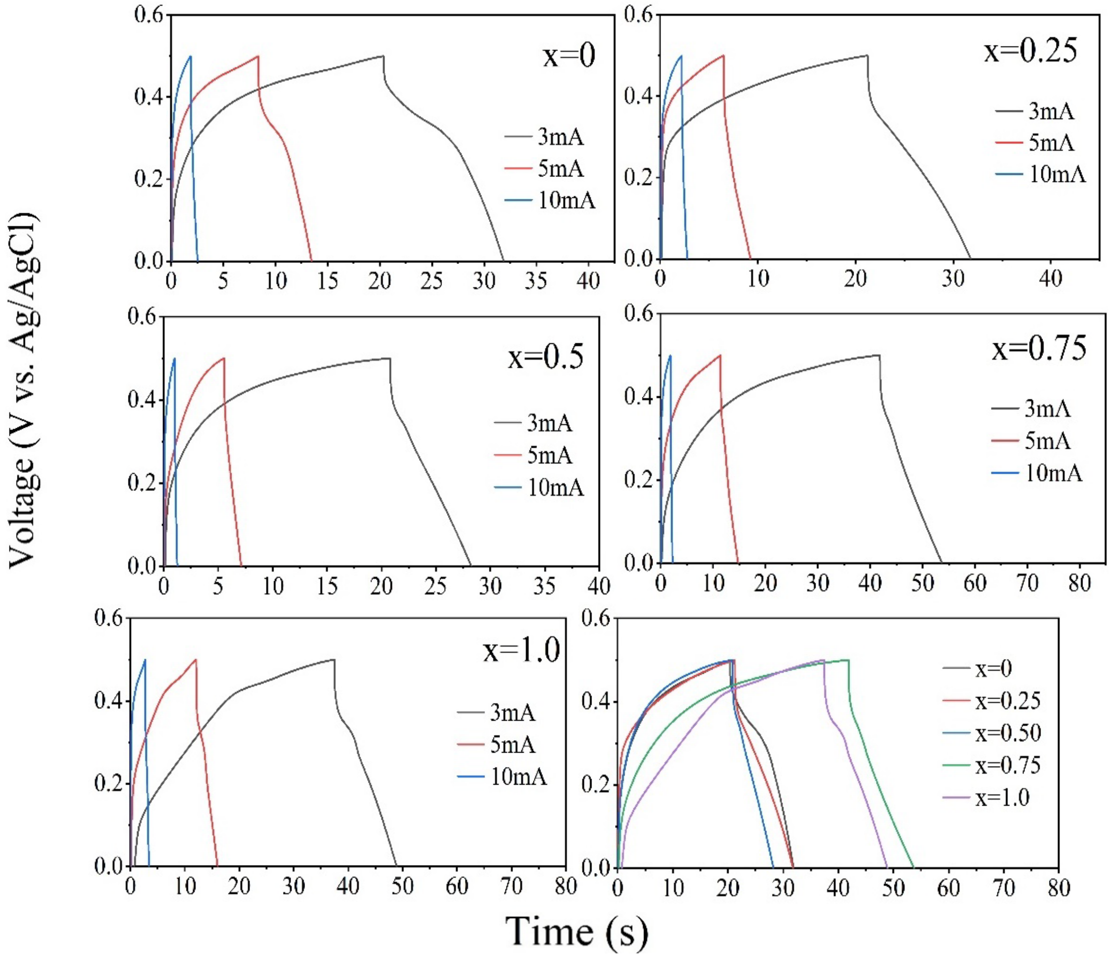

Fig. 6. GCD curve of spinel $ZnNi_xMn_xCo_{2-2x}O_4$ at different x substitutions and their comparison, with a fixed 3 mA/cm² applied current.

Fig. 7 presents the Nyquist plot for five composite materials with varying x values. The resistance values correlate with capacitance; lower resistance facilitates reactions, resulting in higher capacitance [43-44]. Conversely, higher resistance results in lower capacitance due to the difficulty of reactions occurring within the system. The charge transfer resistance (R_{CT}) values indicate this relationship, with smaller curves signifying lower reaction resistance. The lowest resistance occurs at x = 0.75, followed by x = 1.0, x = 0.25, x = 0.50, and x = 0. The lower R_{CT} enhances charge transfer throughout the charge and discharge processes in the supercapacitor, resulting in improved specific capacitance.

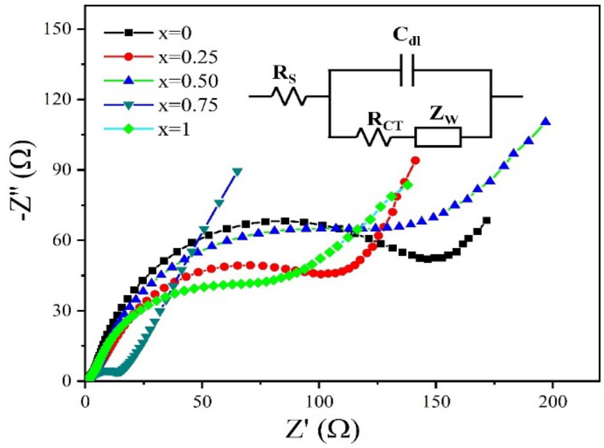

Fig. 7. Nyquist plot of spinel $ZnNi_xMn_xCo_{2-2x}O_4$ *(x = 0, 0.25, 0.50, 0.75, and 1.0) and the suggested model for the internal resistance of electrodes.*

4. Conclusions

$ZnCo_2O_4$, $ZnNiMn_2O_4$, and $ZnNi_xMn_xCo_{2-2x}O_4$ (where x = 0.25, 0.5, 0.75, and 1.0) were studied for supercapacitor electrode application. The single-step hydrothermal method were employed to synthesize all products. The phase of the materials and crystal structure were confirmed through XRD analysis, while elemental composition was determined by XPS analysis. The sample morphology was illustrated using SEM and TEM. All experiments used 2 M KOH electrolyte for the electrochemical properties throughout the experiments. The electrochemical studies revealed that $ZnNi_{0.75}Mn_{0.75}Co_{0.5}O_4$ showed the highest specific capacitance at the 5 mV/s scan rate, and the trends observed in GCD agreed with the CV results. Furthermore, EIS analysis showed the internal resistance of all materials and indicated that the $ZnNi_{0.75}Mn_{0.75}Co_{0.5}O_4$ sample had the lowest internal resistance. This research demonstrates the effectiveness of using substituted compositions in the mixing spinel $ZnNi_xMn_xCo_{2-2x}O_4$ nanomaterial. The improvements found in this work were attributed to the substitution, which led to lower internal resistance and enhanced electrical energy storage capacity.

Acknowledgments

This study was funded by King Mongkut's University of Technology North Bangkok (contract no. KMUTNB-67-KNOW-20).

References

[1] Y. A. Kumar, K. D. Kumar, H-J Kim, Electrochimica Acta **330**, 135261 (2020); https://doi.org/10.1016/j.electacta.2019.135261
[2] J. Mitali, S. Dhinakaran, A.A. Mohamad, Energy Storage and Saving **1**(3), 166 (2022); https://doi.org/10.1016/j.enss.2022.07.002
[3] K. M. Tan, T. S. Babu, V. K. Ramachandaramurthy, P. Kasinathan, S. G. Solanki, S. K. Raveendran, Journal of Energy Storage **39**, 102591 (2021); https://doi.org/10.1016/j.est.2021.102591
[4] A. N. Abdalla, M. S. Nazir, H. Tao, S. Cao, R. Ji, M. Jiang, L. Yao, Journal of Energy Storage **40**, 102811 (2021); https://doi.org/10.1016/j.est.2021.102811
[5] A. A. Kebede, T. Kalogiannis, J. V. Mierlo, M. Berecibar, Renewable and Sustainable Energy Reviews **159**, 112213 (2022); https://doi.org/10.1016/j.rser.2022.112213
[6] P. N. Nikam, S. S. Patil, U. M. Chougale, A. V. Fulari, V. J. Fulari, Journal of Energy Storage **96**, 112648 (2024); https://doi.org/10.1016/j.est.2024.112648
[7] T. Shahanas, J. Yesuraj, G. Harichandran, B. Muthuraaman, K. Kim, Journal of Alloys and Compounds **933**, 167645 (2023); https://doi.org/10.1016/j.jallcom.2022.167645
[8] S. Aouini, A. Bardaoui1, D. M. F. Santos, R. Chtourou, Journal of Materials Science: Materials in Electronics **33**, 12726 (2022); https://doi.org/10.1007/s10854-022-08219-4
[9] S. Aman, S. Gouadria, F. F. Alharbi, M. N. Saeed, H. M. T. Farid, Applied Physics A **129**, 347 (2023); https://doi.org/10.1007/s00339-023-06591-4
[10] S. Fleischmann, J. B. Mitchell, R. Wang, C. Zhan, D. Jiang, V. Presser, V. Augustyn, Chemical Reviews **120**(14), 6738 (2020); https://doi.org/10.1021/acs.chemrev.0c00170
[11] A. N. Alqarni, E. Cevik, M. A. Almessiere, A. Baykal, M. A. Gondal, M. Hassan, A. Bozkurt, A. Iqbal, S. M. Asiri, Y. Slimani, Journal of Physics and Chemistry of Solids **177**, 111288 (2023); https://doi.org/10.1016/j.jpcs.2023.111288
[12] S. B. Narang, K. Pubby, Journal of Magnetism and Magnetic Materials **519**, 167163 (2021); https://doi.org/10.1016/j.jmmm.2020.167163
[13] D. S. Mathew, R.-S. Juang, Chemical Engineering Journal **129**, 51 (2007); https://doi.org/10.1016/j.cej.2006.11.001
[14] S. M. Hoque, Md. A. Choudhury, Md. F. Islam, Journal of Magnetism and Magnetic Materials **251,** 292 (2002); https://doi.org/10.1016/S0304-8853(02)00700-X
[15] C. R. Vestal, Z. J. Zhang, International Journal of Nanotechnology, **1**(1/2), 240 (2004); https://doi.org/10.1504/IJNT.2004.003727
[16] S. Gamal, D. A. Kospa, A. Gebreil, S. A. El-Hakam, A. I. Ahmed, A. A. Ibrahim, International Journal of Hydrogen Energy, **48**(49), 18890 (2023); https://doi.org/10.1016/j.ijhydene.2023.02.024
[17] P. Chomkhuntod, P. Phonsuksawang, A. Waehayee, K. Ngamchuea, P. Iamprasertkun, S. Maensiri, A. Ruangvittayanon, T. Siritanon, Journal of Energy Storage **86**(B), 111303 (2024); https://doi.org/10.1016/j.est.2024.111303
[18] A. Murugan, V. Siva, A. Shameem, R. Deepika, S. Bharathkumarf, H. Valdés, S. A. Bahadur, Journal of Energy Storage **99**(A), 113179 (2024); https://doi.org/10.1016/j.est.2024.113179
[19] S. Kumar, A. Alshoaibi, Ravina, K. Kumari, F. Ahmed, N. M. Shaalan, S. Dalela, R. Kumar, P. A. Alvi, Journal of Electronic Materials **53**(10), 5894 (2024); https://doi.org/10.1007/s11664-024-11059-z
[20] A. Goel, T. T. Mashangva, S. Prasher, A. Sharma, M. Kumar, Journal of Applied Electrochemistry **54**, 2281 (2024); https://doi.org/10.1007/s10800-024-02103-1
[21] M. Ganesan, S. Alagar, V. Bagchi, S. Piraman, Journal of Energy Storage **98**(A), 112954 (2024); https://doi.org/10.1016/j.est.2024.112954
[22] M. Sharma, A. Ahmed, A. Singh, N. Lalotra, A. Dubey, S. Arya, Kamni, Materials Chemistry and Physics Volume **324**, 129676 (2024); https://doi.org/10.1016/j.matchemphys.2024.129676
[23] G. Sivaguru, U. K. Ghorui, M. Girirajan, G. K. Dalapati, P. S. Maram, S. Ghosh, S. Sangaraju, S. Chakrabortty, ACS Applied Energy Materials **7**(17), 7205 (2024); https://doi.org/10.1021/acsaem.4c01087
[24] A. J. C. Mary, A. C. Bose, Applied Surface Science **425**, 201 (2017);

https://doi.org/10.1016/j.apsusc.2017.06.313
[25] M. Sharma, A. Gaur, The Journal of Physical Chemistry C **124**(1), 9 (2020); https://doi.org/10.1021/acs.jpcc.9b08170
[26] R. Balakumar, M. Kanagasabapathy, R. Arunkumar, Electrochimica Acta **497**, 144516 (2024); https://doi.org/10.1016/j.electacta.2024.144516
[27] B. G. Thali, R. M. Kamble, Journal of Solid State Electrochemistry **28**(9), 3297 (2024); https://doi.org/10.1007/s10008-024-05909-3
[28] X. Lei, Y. Zhang, J. Han, Y. Tian, P. Zhao, W. Guo, Y. Zhang, Journal of Power Sources **612**, 234784 (2024); https://doi.org/10.1016/j.jpowsour.2024.234784
[29] C. Li, X. Feng, J. Zhou, G. Zhao, K. Cheng, H. Yu, H. Li, H. Yang, D. Zhao, X. Wang, Metals **14**(8), 84 (2024); https://doi.org/10.3390/met14080841
[30] W. Yang, I. Zhitomirsky, Preparation of ferromagnetic perovskite $La_{0.65}Sr_{0.35}MnO_3$ electrodes for supercapacitor applications, Journal of Materials Science: Materials in Electronics **35**, 1507 (2024). https://doi.org/10.1007/s10854-024-13290-0
[31] A. Afrooze, D. P. M. D. Shaik, Physica Scripta **99**(8), 085993 (2024); https://doi.org/10.1088/1402-4896/ad629a
[32] A. K. Gupta, A. Kumar, M. Marndi, N. K. Giri, R. R. Shahi, Energy Storage **6**(5), e70002 (2024); https://doi.org/10.1002/est2.70002
[33] B. A. A. Jahdaly, A. Abu-Rayyan, M. M. Taher, K. Shoueir, Omega **7**(27), 23673 (2022); https://doi.org/10.1021/acsomega.2c02305
[34] P. Phonsuksawang, P. Khajondetchairit, K. Ngamchuea, T. Butburee, S. Sattayaporn, N. Chanlek, S. Suthirakun, T. Siritanon, Electrochimica Acta **368**, 137634 (2021); https://doi.org/10.1016/j.electacta.2020.137634
[35] H. M. T. Farid, S. Gouadria, S. M. Al-Moayid, H. Algarni, M. Z. Ansari, H. E. Ali, Journal of Energy Storage **66**, 107394 (2023); https://doi.org/10.1016/j.est.2023.107394
[36] J. Shan, C. Shi, H. Zeng, T. Wei, T. Maitisaiyidi, G. Zhu, Y. Zeng, Z. Sun, Journal of Solid State Electrochemistry **28**, 2899 (2024); https://doi.org/10.1007/s10008-024-05845-2
[37] V. T. Tan, L. T. Vinh, T. N. Khiem, H. D. Chinh, Bulletin of Chemical Reaction Engineering & Catalysis **14**(2), 404 (2019); https://doi.org/10.9767/bcrec.14.2.3613.404-412
[38] Y. Köseoğlu, Ceramics International **40**(3), 4673 (2014); https://doi.org/10.1016/j.ceramint.2013.09.008
[39] L. V. Saraf, P. Nachimuthu, M. H. Engelhard, D. R. Baer, Journal of Sol-Gel Science and Technology **53**, 141 (2010); https://doi.org/10.1007/s10971-009-2067-2
[40] S. Agrohiya, S. Dahiya, P. K. Goyal, I. Rawal, A. Ohlan, R. Punia, A. S. Maan, ECS Sensors Plus **1**(4), 043601 (2022); https://doi.org/10.1149/2754-2726/ac973f
[41] M. Jing, H. Hou, Y. Yang, Y. Zhu, Z. Wu, X. Ji, Electrochimica Acta **165**, 198 (2015); https://doi.org/10.1016/j.electacta.2015.03.032
[42] N. A. Hassan, M. H. Al-Timimi, Journal of Ovonic Research **21**, 139-150 (2025); https://doi.org/10.15251/JOR.2025.211.139
[43] T. Kansaard, T.Singha, S. Wannapop, A. Boonkitkoson, Y. Chuminjak, J. Sodtipinta, A. Somdee, Journal of Alloys and Compounds **1010**, 1781185 (2025); https://doi.org/10.1016/j.jallcom.2024.178185
[44] A. Somdee, T. Kanssard, T. Singha, Digest Journal of Nanomaterials and Biostructures **20**, 113-119 (2025); https://doi.org/10.15251/DJNB.2025.201.113